Short-time-delay limit of the self-coupled FitzHugh-Nagumo system

Thomas Erneux,[1] Lionel Weicker,[2,3] Larissa Bauer,[4] and Philipp Hövel[4,5,*]

[1]*Université Libre de Bruxelles, Optique Nonlinéaire théorique, Campus Plaine, C.P. 231, 1050 Bruxelles, Belgium*

[2]*LMOPS, CentraleSupélec, Université Paris-Saclay, 57070 METZ*

[3]*LMOPS, CentraleSupélec, Université de Lorraine, 57070 METZ*

[4]*Institut für Theoretische Physik, Technische Universität Berlin, Hardenbergstraße 36, 10623 Berlin, Germany*

[5]*Bernstein Center for Computational Neuroscience Berlin, Humboldt-Universität zu Berlin, Philippstraße 13, 10115 Berlin, Germany*

(Received 18 December 2015; published 12 February 2016)

We analyze the FitzHugh-Nagumo equations subject to time-delayed self-feedback in the activator variable. Parameters are chosen such that the steady state is stable independent of the feedback gain and delay τ. We demonstrate that stable large-amplitude τ-periodic oscillations can, however, coexist with a stable steady state even for small delays, which is mathematically counterintuitive. In order to explore how these solutions appear in the bifurcation diagram, we propose three different strategies. We first analyze the emergence of periodic solutions from Hopf bifurcation points for τ small and show that a subcritical Hopf bifurcation allows the coexistence of stable τ-periodic and stable steady-state solutions. Second, we construct a τ-periodic solution by using singular perturbation techniques appropriate for slow-fast systems. The theory assumes $\tau = O(1)$ and its validity as $\tau \to 0$ is investigated numerically by integrating the original equations. Third, we develop an asymptotic theory where the delay is scaled with respect to the fast timescale of the activator variable. The theory is applied to the FitzHugh-Nagumo equations with threshold nonlinearity, and we show that the branch of τ-periodic solutions emerges from a limit point of limit cycles.

DOI: 10.1103/PhysRevE.93.022208

I. INTRODUCTION

The propagation of electrically excitable signals is essential for the good functioning of the body. In the brain, neurons transfer information to other parts of the brain and body via propagation of action potentials along axons, pacemaker cells ensure proper sequential contraction of parts of the heart to pump blood to all regions of the body, and pancreatic cells undergo bursting electrical activity to secrete insulin to control blood glucose levels [1–3]. The classical example of an excitable phenomenon is the firing of a nerve. According to observations by Hodgkin and Huxley (HH) [1,4], a subthreshold depolarization dies away monotonically, but a super-threshold depolarization is amplified and initiates a spike potential. In the brain, such a transient pulse is on the order of milliseconds and can propagate a single neuron to many receiving neurons. There, incoming signals can collectively cause the target neuron to "fire." FitzHugh and Nagumo (FHN) [5,6] later formulated a two-variable caricature of the HH model equations that possess many similar dynamical properties. The FHN model is quite useful as a minimum system for a systematical analysis of the effects of delayed feedbacks in neurosystems [7–10].

Delays are inherent in neuronal networks due to finite conduction velocities and synaptic transmission times. Neurons with short axons transmit over small distances of less than 1 mm at velocities below 2 m/s. Long axons transmit over larger distances (centimeters to meters) at velocities of 10–100 m/s [11]. Specific synchronization or desynchronization patterns are essential for neural functioning and have been investigated by formulating network models [12,13]. Biologically realistic network models have been recently explored showing how time delays affect the structural heterogeneity of the network [14–17]. While most studies concentrated on populations of coupled limit-cycle oscillators, work has also been done on coupled excitable units [18–20]. The case of two delayed coupled FHN systems has been examined in detail showing that stable periodic oscillations may coexist with a stable steady state [21–23]. The delayed coupling enables the sequential spiking of the two cells by controlling the timing of each pulse. In this particular configuration, the period is close to twice the delay τ. In Ref. [24], we applied asymptotic techniques appropriate for slow-fast systems and constructed periodic solutions of a two delayed-coupled FHN system. We found that in addition to the 2τ-periodic solution, stable $2\tau/n$-periodic solutions ($n = 1,2,...$) are possible for the same parameter values. This raised the fundamental question of whether stable periodic and steady states may coexist in the case of a single time-delayed FHN system, which is also called self-coupled FHN system. We recently investigated this problem with $\tau = O(1)$ fixed. We found that indeed stable τ/n-periodic oscillations are possible and emerge from limit points of limit cycles [25]. Experiments using an electronic circuit modeled by the same FHN equations showed that they are robust to noise.

The main objective of this paper is to determine if a small delay is enough to generate such τ-periodic solutions, which is mathematically counterintuitive (cf. Sec. 4.4, p. 48, of Ref. [26]). Specifically, we consider the following FHN equations:

$$\varepsilon \dot{x} = x - \frac{x^3}{3} - y + c[x(t-\tau) - x], \tag{1a}$$

$$\dot{y} = x + a, \tag{1b}$$

*phoevel@physik.tu-berlin.de

where the variables x and y represent the membrane potential and an inactivation variable, i.e., an activator and inhibitor, respectively. The fixed parameter $\varepsilon \ll 1$ implies that x is a fast variable compared to y, and a is a control parameter. The last term in the right-hand side of Eq. (1a) models the delayed synaptic feedback acting as a membrane current. The feedback gain c is positive (negative), if the synapse is excitatory (inhibitory). Since the current is ionic, we assume that its magnitude will be roughly proportional to the difference $x(t-\tau)-x(t)$. Finally, the current will occur after a finite delay due to the finite conduction velocity of the nerve axons and due to the synaptic delay.

First investigations of Eqs. (1) started with Plant [27] who examined the effect of the feedback term $c[x(t-\tau)-x_0]$, where $x_0=-a$ is the steady-state value. Plant considered parameters such that the system with no feedback has a stable equilibrium point ($a^2 \geqslant 1$) and showed that this stability is maintained for the system with feedback and sufficiently small delay. He then showed that when $c<0$, i.e., the recurrent feedback is inhibitory, there is a Hopf bifurcation at a critical value of the delay that leads to oscillations. More recently, the delayed FHN problem was studied with the feedback function in the right-hand side of the inhibitor Eq. (1b) instead of Eq. (1a) and with noise [28–30]. Again, parameters were chosen such that the system is at a stable resting state without feedback and noise. Noise-induced oscillations are, however, possible giving rise to coherence resonance, where the feedback gain and the delay are able to enhance or diminish this effect.

In this paper, we analyze Eqs. (1) when the steady state is stable independent of the values of $c>0$ and τ in the parameter range $a^2>1$, that is, in the excitable regime. In Ref. [31], the authors investigated Eqs. (1) with $c<0$ and determined the possible routes to chaos [32]. But if $c<0$, the stable steady state of the nondelayed FHN system undergoes a Hopf bifurcation as soon as $c\neq 0$ and negative. Here, we exclusively concentrate on a stable steady stable that remains linearly stable in the presence of a delayed feedback. Our objective is to demonstrate both analytically and numerically that a small delay is enough to induce stable oscillations coexisting with a stable steady state. We propose three different strategies to determine these solutions. (i) We analyze the Hopf bifurcations if a^2 is less but close to 1 and the time delay τ is small. Stable τ-periodic solutions may indeed coexist with a stable steady state through a subcritical Hopf bifurcation followed by a limit-point of limit-cycles (or saddle node of limit cycles). If a^2 is now slightly increased and passes 1, the Hopf bifurcation point moves to infinity but we may reasonably expect that the limit point of limit cycles persists. This idea is explored by determining the bifurcation diagram of the periodic solutions using a numerical continuation method. (ii) We construct the nearly τ-periodic solution for $a^2>1$, $\tau=O(1)$ in the limit ε small by using a method appropriate for slow-fast systems. It is not a routine application of singular-perturbation techniques because we are dealing with delay differential equations (DDEs). We then investigate the validity of our approximations as $\tau\to 0$ by comparing analytical and numerical bifurcation diagrams. (iii) We propose an asymptotic theory of the periodic solutions based on the limits ε and $\tau=O(\varepsilon)$ being small. Our goal is to demonstrate that these solutions terminate at a limit point of limit cycles.

The paper is organized as follows. In Sec. II, we analyze the Hopf bifurcations assuming $a<1$, $|a-1|=O(\varepsilon)$, and $\tau=O(\varepsilon)$ or $\tau=O(\sqrt{\varepsilon})$. Combining analytical and numerical techniques, we show that there is indeed a branch of stable τ-periodic solutions that overlaps a stable steady state. In Sec. III, we consider $a>1$ and determine τ-periodic solutions by direct numerical integration starting from selected initial conditions. The limit-cycle oscillations are found to be relaxation oscillations that we explore in the phase plane by singular-perturbation techniques. The slow outer solution is relatively simple to determine but the construction of the inner or fast transition layer solutions is mathematically difficult. These problems are solved by considering the limit of large values of the feedback gain c. In Sec. IV, we propose a full analytical study of the bifurcation diagram based on the limits ε and $\tau=O(\varepsilon)$ small. We apply the theory for the FHN equations with threshold nonlinearity. Finally, we discuss in Sec. V the physical impact of our results for delayed slow-fast systems and the interest of developing analytical tools for DDEs.

II. HOPF BIFURCATION

The FHN model described by Eqs. (1) has one single steady state $x=-a$ and $y=-a+a^3/3$, and from the linearized theory, we determine the following characteristic equation

$$\varepsilon\lambda^2-\lambda[1-a^2+c(e^{-\lambda\tau}-1)]+1=0. \tag{2}$$

By considering $\lambda=i\sigma$, we obtain the two following Hopf conditions by separating Eq. (2) in real and imaginary part:

$$-\varepsilon\sigma^2-\sigma c\sin(\sigma\tau)+1=0, \tag{3a}$$

$$1-a^2-2c\sin^2(\sigma\tau/2)=0. \tag{3b}$$

Equation (3b) indicates that a Hopf bifurcation is only possible if $a^2\leqslant 1$ and $c>0$. The three first Hopf bifurcation lines in the (τ,a) plane are shown in Fig. 1 as τ_{H_0}, τ_{H_1}, and τ_{H_2}. These curves will be discussed in detail next.

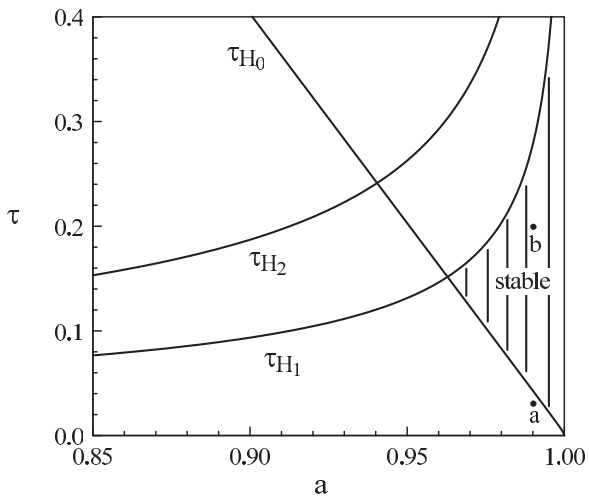

FIG. 1. Hopf bifurcation curves for small τ and a close to 1. Only the cross-hatched region corresponds to a stable steady state. Parameters: $\varepsilon=0.03$ and $c=10$.

We wish to determine asymptotic approximations of the Hopf bifurcation lines in the (a,τ) parameter plane, assuming $|a-1| = O(\varepsilon)$ and $\tau = O(\varepsilon^p)$, where $p > 0$. If $|a-1| = O(\varepsilon)$, Eq. (3b) implies that $|\sin(\sigma\tau/2)| = O(\varepsilon^{1/2})$. The obvious case is to consider $\sigma\tau/2 = O(\varepsilon^{1/2})$. All three terms in Eq. (3a) are then of the same order of magnitude if $\sigma = O(\varepsilon^{-1/2})$. This defines a first limit. There is, however, another limit that is much more subtle to detect. $|\sin(\sigma\tau/2)| = O(\varepsilon^{1/2})$ in Eq. (3b) is again verified if $\sigma\tau/2 = \pi n + O(\varepsilon^{1/2})$, where $n = 1,2,...$ The first and last terms in Eq. (3a) still motivates the scaling $\sigma = O(\varepsilon^{-1/2})$. It defines the second limit. The determination of the leading approximations for the two cases is detailed in the Appendix. In summary, the first Hopf bifurcation satisfies

$$\text{I:}\quad a-1 = -\frac{\varepsilon c(\tau/\varepsilon)^2}{4(1+c\tau/\varepsilon)} \text{ and } \sigma = \sqrt{\frac{1}{\varepsilon(1+c\tau/\varepsilon)}}, \quad (4)$$

with $\tau/\varepsilon = O(1)$. It is the line that emerges from $(a,\tau) = (1,0)$ and labeled by τ_{H_0} in Fig. 1. Other Hopf bifurcations, which are labeled by τ_{H_n} (displayed for $n = 1,2$), occur for

$$\text{II:}\quad a-1 = -\frac{\varepsilon(1-\sigma_0)^2}{4\sigma_0^2 c} \text{ and } \sigma = \frac{\sigma_0}{\sqrt{\varepsilon}}, \quad (5)$$

with $\sigma_0 = 2n\pi\sqrt{\varepsilon}/\tau$ $(n = 1,2,...)$ and $\tau/\sqrt{\varepsilon} = O(1)$. They are shown as the hyperbolic lines in Fig. 1 for $n = 1,2$. A similar analysis of the solutions of the characteristic Eq. (2) for small ε, $|a-1| = O(\varepsilon)$, and $\tau = O(\varepsilon)$ or $\tau = O(\sqrt{\varepsilon})$ indicates that the steady state is linearly stable only in the cross-hatched region bounded by τ_{H_0} and τ_{H_1} in Fig. 1.

We investigate the stability diagram by perturbing the steady state in two different ways:

$$\text{(i)}\quad x = -a \quad \text{for} \quad -\tau < t < 0, \quad (6a)$$

$$y(0) = -a + a^3/3 + 10^{-3}, \quad (6b)$$

and

$$\text{(ii)}\quad x(t) = 1.5\cos[2\pi(t+\tau)/\tau] \quad \text{for} \quad -\tau < t < 0, \quad (7a)$$

$$y(0) = -a + a^3/3 + 10^{-3}. \quad (7b)$$

We fix $a = 0.99$ and consider different values of τ. We integrate the FHN equations for a time interval of 16000τ. We find that (x,y) trajectory approaches the stable steady state under conditions (i) if $\tau_{H0} < \tau < \tau_{H1}$. If τ is slightly below τ_{H0}, the steady state is unstable [point (a) in Fig. 1] and the system approaches a low-frequency periodic solution as shown in Fig. 2(a). On the other hand, if we consider the second set of initial conditions, we observe that slow-fast oscillation of period close to τ coexist with the stable steady state as depicted, e.g., in Fig. 2(b) for parameters marked by point b $(a = 0.99, \tau = 0.2)$ in Fig. 1.

In order to explore the bifurcation diagram of the periodic solutions in more detail, we use the continuation method DDE-BIFTOOL varying the time delay [33]; see Fig. 3. The bifurcation at τ_{H_0} is clearly supercritical and the amplitude grows parabolically as τ decreased from τ_{H_0}. Close to $\tau = 0$, the amplitude increases dramatically. This can be anticipated since the delay has no effects if $c\tau < O(\varepsilon)$ and the DDE problem reduces to an ordinary differential FHN equation

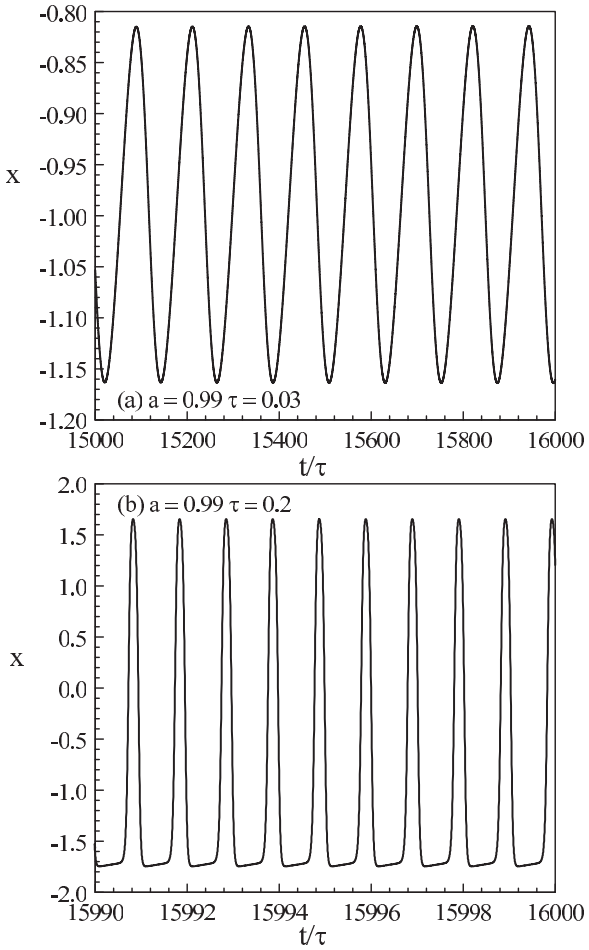

FIG. 2. Stable long-time periodic solution. Panel (a) shows nearly harmonic oscillations with a period proportional to $\varepsilon^{1/2}$ in units of time t ($\varepsilon^{-1/2}$ in units of time t/τ). Panel (b) shows a large-amplitude periodic solution of period τ (of period 1 in units of time t/τ). Parameters as marked by points a and b in Fig. 1.

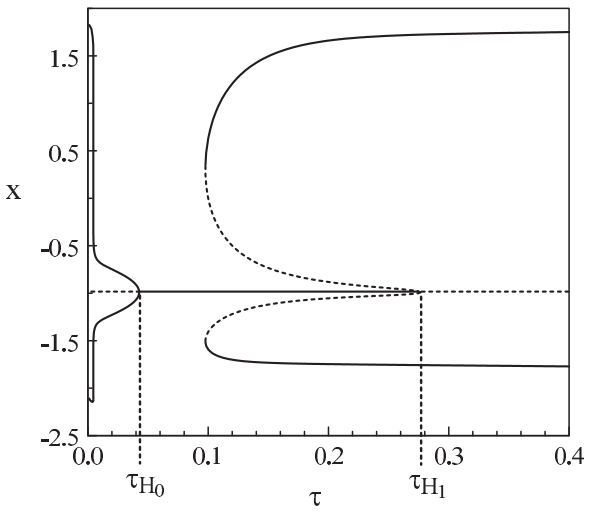

FIG. 3. Bifurcation diagram of the periodic solutions. The extrema of x are shown as a function of τ. Dashed and solid lines correspond to unstable and stable solutions, respectively. Parameters: $a = 0.99$, $\varepsilon = 0.03$, and $c = 10$.

admitting relaxation oscillations. On the other hand, the bifurcation at $\tau = \tau_{H_1}$ is subcritical and leads to stable high-amplitude, pulsating solutions after the branch of periodic solutions folds back. DDE-BIFTOOL also provides the period of the solutions. The upper branch starting near $\tau = 0.1$ shows a period almost equal to τ.

If $a < 1$ is now increased and passes 1, τ_{H0} and its Hopf bifurcation branch disappear from the diagram and τ_{H_1} moves to infinity. We may, however, reasonably expect that the limit point of limit cycles persists for $a > 1$. In summary, the determination of the bifurcation diagram for a slightly less than $a = 1$ provides insights on the diagram for a slightly larger than $a = 1$ by exhibiting a limit point of limit cycles.

III. RELAXATION OSCILLATIONS

We now consider $a > 1$ and seek a stable τ-periodic solution coexisting with the stable steady state. Using a cosine function of period τ as the initial function for x in the interval $(-\tau \leqslant t < 0)$, we obtain a stable limit-cycle solution in the phase plane (x, y); see Fig. 4(a). Although the limit cycle is symmetric with respect to the line $y = 0$, the time spent along the left and right branches of the S-shaped nullcline,

$$y = f(x) \equiv x - \frac{x^3}{3}, \tag{8}$$

is different; see Fig. 4(b) for $\tau = 2$. As we progressively decrease τ, the extrema of y, denoted by y_2 and y_1 in Fig. 4(a), approach the line $y = 0$. We wish to determine the bifurcation diagram of these oscillations as τ approaches zero. To this end, we look for a T-periodic solution with T as close to τ as

$$T = \tau + \varepsilon\delta, \tag{9}$$

where $\delta = O(1)$ if $\varepsilon \to 0$. The limit cycle in the phase plane y versus x follows the right and left branches of the slow manifold $y = f(x)$ defined by Eq. (8). These slowly varying parts are connected by fast-transition layers located at $y = y_1$ and $y = y_2$, $(y_1 < y_2)$. Using Eq. (1b) and the fact that $y = f(x)$ along the slow manifold, we compute the leading contribution of the period $T = \tau$. Specifically, we determine the travel times along the left and right branches of $y = f(x)$

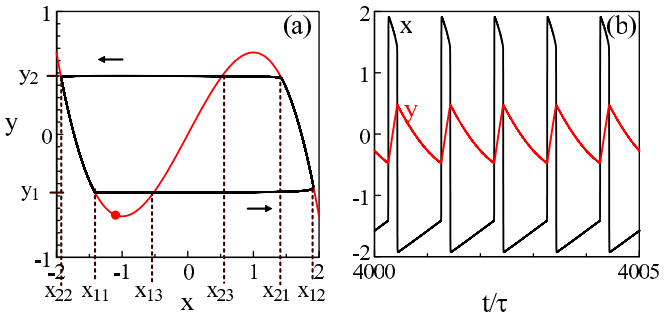

FIG. 4. Panel (a): Periodic orbit in the phase plane. The limit cycle is the long time solution of Eqs. (1). The red S-shaped curve is the slow manifold $y = f(x)$ and the dot is the stable steady state. The initial conditions are $x = \cos(2\pi t/\tau)$ for $-\tau \leqslant t < 0$ and $y(0) = 0$. Panel (b): Time evolution of x and y. The period is nearly equal to τ. Parameters: $a = 1.1$, $\varepsilon = 0.03$, $\varepsilon = 5 \times 10^{-3}$, $c = 10$, and $\tau = 2$.

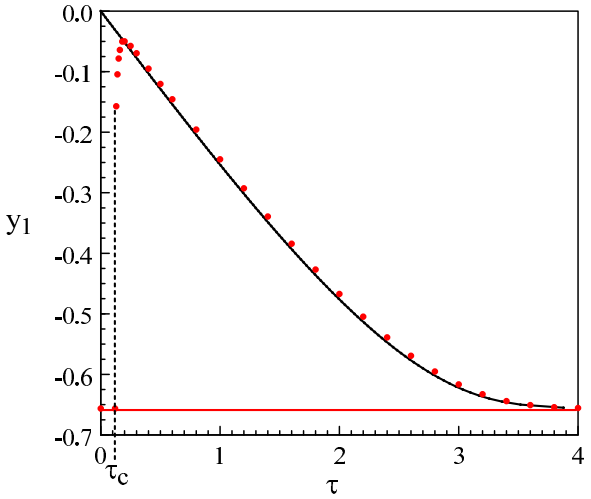

FIG. 5. Minimum of y as function of τ. The solid black line is the approximation Eq. (12). The red (gray) dots are obtained by numerical integration of Eqs. (1). Parameters: $a = 1.1$, $c = 10$, and $\varepsilon = 0.03$.

and formulate the condition

$$T = \tau = \int_{x_{12}}^{x_{21}} \frac{f'(x)dx}{x + a} + \int_{x_{22}}^{x_{11}} \frac{f'(x)dx}{x + a}. \tag{10}$$

Note that the real roots of $y - f(x) = 0$ can be determined using Viète's trigonometric expression of the roots in the three-real-roots case $(y^2 \leqslant 2/3)$. They are given by $(u_0 \geqslant u_1 \geqslant u_2)$,

$$u_k = 2\cos\left[\frac{1}{3}\arccos\left(-\frac{3y}{2}\right) - k\frac{2\pi}{3}\right], \tag{11}$$

with $-\pi \leqslant \arccos(u) \leqslant \pi$ and $k = 0, 1, 2$. We next anticipate our analysis of the transition layers and assume that $y_1 = -y_2$. Since $f(x)$ is an odd function, we realize that $x_{21} = -x_{11} = -u_2$ and $x_{22} = -x_{12} = -u_0$. We calculate the integrals in Eq. (10) and find

$$\tau = u_0^2 - u_2^2 - (a^2 - 1)\ln\left(\frac{a^2 - u_2^2}{a^2 - u_0^2}\right). \tag{12}$$

Figure 5 compares the function $\tau = \tau(y_1)$ with numerical estimates obtained from direct simulations of Eqs. (1) added as dots. There is a critical value of τ, denoted by τ_c, below which no limit cycles have been found numerically. The slow-fast construction of the limit cycle fails in the limit $\tau \to 0$ because there is no more a clear separation of time scales. We observe that the minimum decreases slightly before τ approaches $\tau_c \simeq 0.13$. On the other hand, we find $y_1 \to f(-a) \simeq -0.66$ as $\tau \to \infty$, which can be expected since the limit-cycle oscillations will spent more and more time near the stable steady state $(x, y) = (-a, f(-a))$ before jumping to the right branch of the slow manifold.

Note that our analysis of the slowly varying parts does not provide $\varepsilon\delta$, i.e., the correction of the main period $T = \tau$. To calculate this correction, we need to consider the fast-transition layer near $y = y_1, y_2$. To this end, we rescale Eqs. (1) by

$$s \equiv t/\varepsilon \tag{13}$$

and note that

$$x(t-\tau) = x(t-T+\varepsilon\delta) = x(t+\varepsilon\delta) = x(s+\delta). \quad (14)$$

The transition-layer equation is then given by

$$x' = f(x) - y + c[x(s+\delta) - x], \quad (15a)$$

$$y' = \varepsilon(x+a), \quad (15b)$$

where prime refers to differentiation with respect to time s. The limit $\varepsilon \to 0$ yields $y' = 0$ implying that $y = y_1, y_2$ are constants in first approximation. Equation (15a) thus becomes

$$x' = f(x) - y_j + c[x(s+\delta) - x], \quad (16)$$

with $j = 1,2$. This equation must satisfy the boundary conditions

$$\lim_{s\to-\infty} x(s) = x_1 \text{ and } \lim_{s\to\infty} x(s) = x_2. \quad (17)$$

Equation (16) is an equation that contains $x(s+\delta)$, where δ is the unknown correction of the period. We assume that there exists a unique value of δ such that Eq. (16) admits a solution satisfying the boundary conditions Eq. (17). For $y = y_1$, the transition layer solution goes from $x = x_{11} < 0$ to $x = x_{21} > 0$, while for $y = y_2 > 0$, the transition layer solution starts from $x = x_{21} > 0$ and moves to $x_{22} < 0$; see Fig. 4. Under the assumption of a symmetry in the inhibitor levels,

$$y_2 = -y_1, \quad (18)$$

the two transition layer equations are identical due to $x_{21} = -x_{11}$ and $x_{22} = -x_{12}$. This is consistent with the fact that δ appears in both transition layer equations.

We cannot solve Eq. (16) analytically because of the advance argument, but we may look for an asymptotic solution in the limit of large values of c. The idea is to reduce the transition layer equation to a second-order ordinary differential equation that we can solve. A similar idea has been successfully used in another delay differential problem [20]. Specifically, we assume that $\delta \to 0$ as $c \to \infty$ and expand $x(s+\delta)$ as

$$x(s+\delta) = x + \delta x' + \frac{\delta^2}{2}x'' + O(\delta^3 x'''). \quad (19)$$

Inserting expansion Eq. (19) into Eq. (16) with $y = y_1$, we obtain after some simplifications

$$0 = \frac{c\delta^2}{2}x'' + (c\delta - 1)x' + f(x) - y_1 + O(c\delta^3 x'''). \quad (20)$$

We eliminate the coefficient multiplying x'' by introducing a new, rescaled time variable,

$$\zeta \equiv \frac{s}{\sqrt{c\delta^2/2}}. \quad (21)$$

Equation (20) then becomes

$$x'' + \frac{(c\delta - 1)}{\sqrt{c\delta^2/2}}x' + f(x) = y_{1,2} + O\left(\frac{c\delta^3}{(c\delta^2)^{3/2}}x'''\right), \quad (22)$$

where prime now means differentiation with respect to ζ. We now seek a solution for δ of the form

$$\delta = c^{-1} + c^{-3/2}\frac{\alpha}{\sqrt{2}} + \ldots, \quad (23)$$

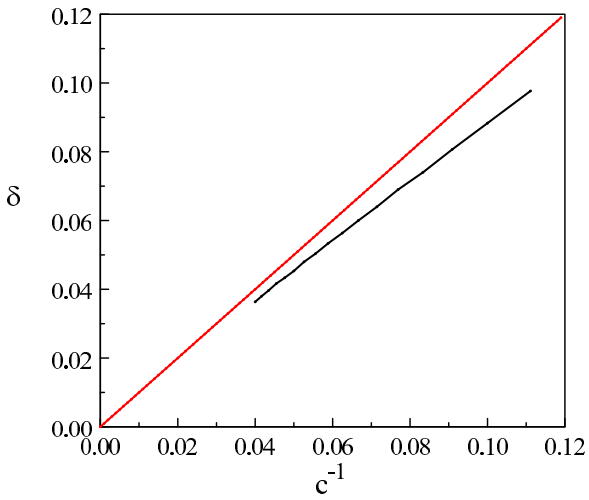

FIG. 6. Correction δ to the period in dependence on the inverse coupling strength c. The red (gray) diagonal line $\delta = 1/c$ is added as a guide to the eye. Same parameters as described in the caption of Fig. 5.

where $\alpha = O(1)$ needs to be determined. The leading behavior of $\delta = c^{-1}$ as $c \to \infty$ has been checked by accurate numerical simulations; see Fig. 6, where the value of δ is determined numerically by first obtaining the correction of the period from τ ($\varepsilon\delta = T - \tau$) and then by dividing this correction by ε. The data progressively approach the straight line as $1/c$ decreases, i.e., for increasing coupling strength. This motivates the asymptotic analysis of Eq. (16) for $c \to \infty$.

Inserting Eq. (23) into Eq. (22) then leads to

$$x'' + \alpha x' + f(x) = y_1 + O(c^{-1/2}). \quad (24)$$

In the limit $c \to \infty$, we neglect the $c^{-1/2}$ correction term and verify that ζ defined by Eq. (21) reduces to $\zeta = \sqrt{2c}s$, which is still a fast time variable as $c \to \infty$. Equation (24) is now a second-order nonlinear ordinary differential equation. The challenge now is to determine α so that Eq. (24) admits a heteroclinic trajectory connecting x_{11} at $\zeta = -\infty$ to x_{12} at $\zeta = \infty$. Equation (24) admits a solution of the form

$$x = x_{11} + \frac{x_{12} - x_{11}}{1 + \exp(A\zeta)}, \quad (25)$$

where $A < 0$. Inserting this expression into Eq. (24), we find

$$A = -\sqrt{\frac{1}{6}}|x_{11} - x_{12}| \quad (26)$$

and

$$\alpha = \sqrt{\frac{1}{6}}(x_{11} + x_{12} - 2x_{13}). \quad (27)$$

In summary, we have determined an asymptotic approximation of the limit cycle for $\tau = O(1)$ by exploring the limit $\varepsilon \to 0$. The approximation is in excellent agreement with the solutions obtained numerically even if $\tau < 1$. It fails if $\tau = O(\varepsilon)$, which can be expected because the assumption of two distinct time scales, namely $T_1 = O(\tau)$ and $T_2 = O(\varepsilon)$ is no more valid. Figure 7 shows the numerical limit cycles close to their limit point located at $\tau_c = 0.13$. We note that

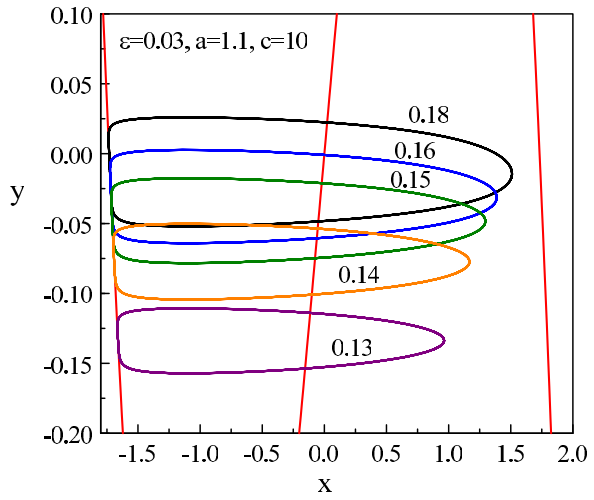

FIG. 7. Limit cycles close to the critical delay where the stable steady state is the only solution. The value of τ is indicated in the figure. Other parameters are the same as described in the caption of Fig. 5.

their orbits are losing contact with the right branch of the slow manifold and that they become asymmetric with respect to the line $y = 0$.

IV. ASYMPTOTIC THEORY WITH $\tau = O(\varepsilon)$ AND $\varepsilon \to 0$

Equations (1) belong to the family of FHN systems of the form

$$\varepsilon x' = f(x,x(t-\tau)) - y, \tag{28a}$$

$$y' = g(x,a), \tag{28b}$$

where the function $y = f(x,x)$ is S shaped and $g(x,a)$ is monotone in the phase plane (x,y). Introducing the fast time s and the rescaled time delay γ defined as

$$s \equiv t/\tau \quad \text{and} \quad \gamma \equiv \varepsilon^{-1}\tau, \tag{29}$$

Eq. (28) can be rewritten as

$$\gamma^{-1}x' = f(x,x(s-1)) - y, \tag{30a}$$

$$y' = \varepsilon\gamma(x+a), \tag{30b}$$

where prime now means differentiation with respect to time s. We next seek a periodic solution of the form

$$x = x_0(s) + \varepsilon x_1(s) + ..., \tag{31a}$$

$$y = y_0(s) + \varepsilon y_1(s) + ... \tag{31b}$$

Inserting Eqs. (31) into Eqs. (30) and equating to zero the coefficients of each power of ε lead to a sequence of problems for the unknown functions x_0, x_1, y_0, y_1,...The first three problems are given by

$$O(1) : \gamma^{-1}x_0' = f(x_0,x_0(s-1)) - y_0, \tag{32a}$$

$$y_0' = 0, \tag{32b}$$

$$O(\varepsilon) : y_1' = \gamma(x_0 + a). \tag{32c}$$

Equation (32b) implies that y_0 is an unknown constant. We then determine a P-periodic solution for x_0 by solving Eq. (32a). The period P is a function of y_0 and we need an additional equation for its determination. Equation (32c) admits a bounded solution for y_1 provided that the right-hand side satisfies the solvability condition

$$\int_0^P (x_0 + a)ds = 0. \tag{33}$$

The problem for x_0 is a nonlinear DDE, which cannot be solved analytically. To progress further, we first consider the approximating case

$$f(x,x(t-\tau)) = -1 - x + 2H(x(t-\tau)), \tag{34a}$$

$$g(x,a) = x + a, \tag{34b}$$

where $H(x)$ is the Heaviside function. Since the function $f(x,x(t-\tau))$ reduces to two distinct linear functions of x depending on the sign of $x(t-\tau)$, we may solve the equation for x_0 analytically. We consider $a > 0$ and the steady state $(x,y) = (-a, -1+a)$ is always stable. Figure 8 shows a stable periodic solution of Eqs. (28) with the functions (34) coexisting with a stable steady state. The initial conditions are $x = \cos(2\pi t/\tau)(-1 < t/\tau \leqslant 0)$, $y(0) = 0$. The solution exhibits a period close to τ and because $\tau < 1$, the limit cycle in the phase plane spends little time near the slow manifold,

$$y = -1 - x + 2H(x), \tag{35}$$

which is added as straight lines in Figs. 8(a) and 8(b). Similar to the continuous FHN system, we note that a periodic solution is no more possible below a critical value of τ.

We now propose to solve Eq. (32a). Figure 9 is an enlargement of Fig. 8(c) showing both $x(s)$ and $x(s-1)$. $x(s-1)$ is zero at $s = 0$, s_1, and s_2. $x(s)$ is zero at $s = \delta$ and $s_1 + \delta$. The period is $s_2 \equiv t_2/\tau = 1 + \delta$ and the interval during which $x(s-1)$ is positive is $s_1 \equiv t_1/\tau = 0.486$. The time lag between $x(s)$ and $x(s-1)$ is $\delta = 0.083$. We identify two distinct regions corresponding to the interval $0 < s < s_1$, where $x(s-1) > 0$, and the interval $s_1 < s < s_2$, where $x(s-1) < 0$.

Next, we solve Eq. (32a) for each part. During the interval $0 < s < s_1$ with $x_0(s-1) > 0$, Eq. (32a) reduces to

$$\gamma^{-1}x_0' = -y_0 + 1 - x_0, \tag{36}$$

which admits the solution

$$x_0 = A\exp(-\gamma s) + 1 - y_0, \tag{37}$$

where A is an integration constant. During the interval $s_1 < s < s_2$ with $x_0(s-1) < 0$, Eq. (32a) simplifies as

$$\gamma^{-1}x_0' = -y_0 - 1 - x_0. \tag{38}$$

It admits the solution

$$x_0 = -1 - y_0 + B\exp(-\gamma(s - s_1)), \tag{39}$$

where B is a new integration constant. We determine A and B by requiring that the solution Eqs. (37) and (39) are equal at

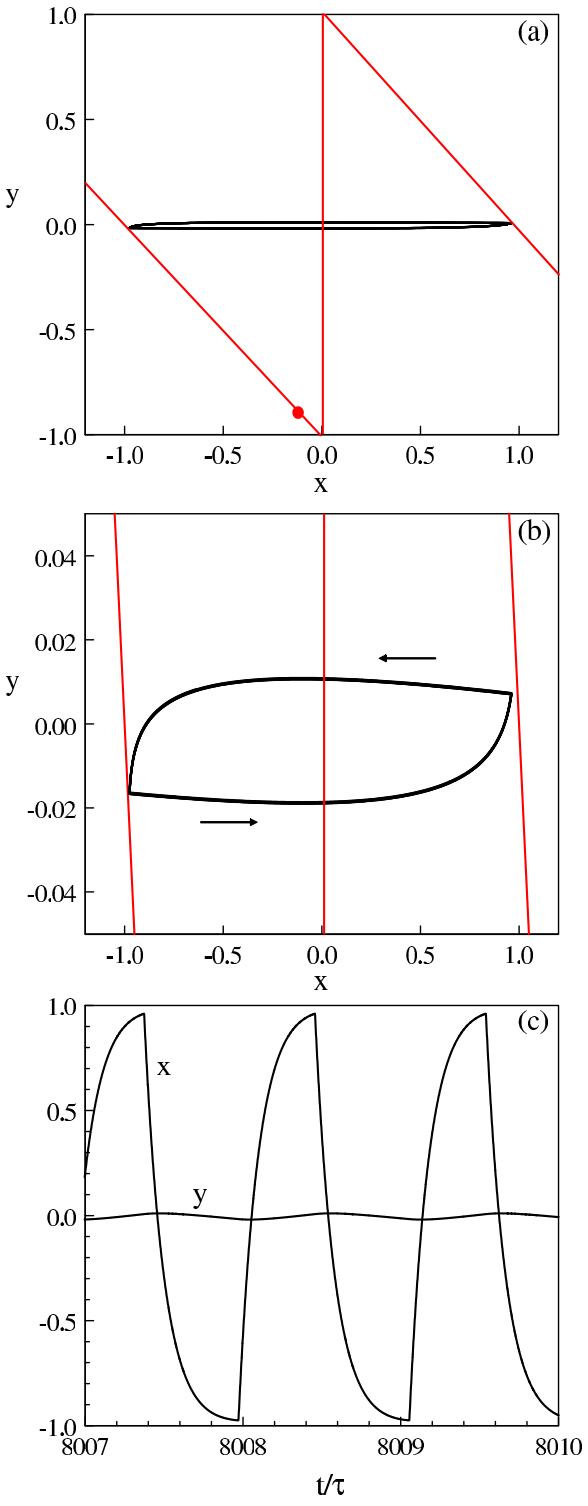

FIG. 8. Stable time-periodic solution of Eqs. (28) with Eqs. (34). Parameters: $\varepsilon = 0.01$, $a = 0.1$, and $\tau = 0.08$. (a) Phase plane (x, y) showing the periodic orbit, the red (gray) piecewise linear nullcline (35), and the stable steady state at $x = -a$. (b) Blow up of the limit cycle shown in (a). Note that the amplitude of y is small but that its average is slightly negative. (c) Time evolution of x and y.

$s = s_1$ and $s = s_2$. We obtain the two conditions given by

$$1 + A\exp(-\gamma s_1) = B - 1, \tag{40a}$$

$$-1 + B\exp(-\gamma s_{21}) = 1 + A, \tag{40b}$$

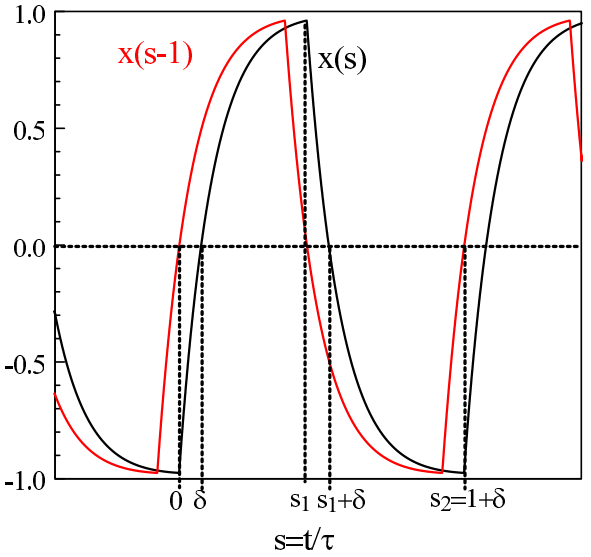

FIG. 9. Time evolution of $x(s)$ and $x(s-1)$ as black and red (gray) curves, respectively. The interval during which $x(s-1)$ is positive is $s_1 \equiv t_1/\tau = 0.486$ and the time lag between $x(s)$ and $x(s-1)$ is $\delta = 0.083$. The period is $s_2 \equiv t_2/\tau = 1 + \delta$. Parameters as described in the caption of Fig. 8.

with $s_{21} = s_2 - s_1$, respectively. Solving these equations for A and B, we obtain

$$A = \frac{-2 + 2\exp(-\gamma s_{21})}{1 - \exp(-\gamma s_2)}, \tag{41a}$$

$$B = \frac{2 - 2\exp(-\gamma s_1)}{1 - \exp(-\gamma s_2)}. \tag{41b}$$

We next use the fact that $x(\delta) = x(s_1 + \delta) = 0$. Via Eq. (37) with $x(\delta) = 0$ and Eq. (39) with $x(s_1 + \delta) = 0$, we obtain two conditions:

$$1 - y_0 + A\exp(-\gamma\delta) = 0, \tag{42a}$$

$$-1 - y_0 + B\exp(-\gamma\delta) = 0. \tag{42b}$$

Inserting the expressions of A and B given by Eqs. (41) into Eqs. (42), we obtain the following two equations for s_1 and δ:

$$1 - y_0 + \frac{-2 + 2\exp(-\gamma(1 + \delta - s_1))}{1 - \exp(-\gamma(1 + \delta))}\exp(-\gamma\delta) = 0, \tag{43a}$$

$$-1 - y_0 + \frac{2 - 2\exp(-\gamma s_1)}{1 - \exp(-\gamma(1 + \delta))}\exp(-\gamma\delta) = 0, \tag{43b}$$

where we have used $s_2 = 1 + \delta$. Subtracting Eqs. (43) leads to an equation without y_0 but relating s_1 and δ. This equation can be reformulated as a quadratic equation for $\exp(-\gamma\delta)$ of the form

$$e^{-2\gamma\delta}e^{-\gamma(1-s_1)} + e^{-\gamma\delta}(-e^{-\gamma} - 2 + e^{-\gamma s_1}) + 1 = 0. \tag{44}$$

Finally, we consider the integral condition Eq. (33) together with Eq. (34b) by using the solution Eqs. (37) and (39)

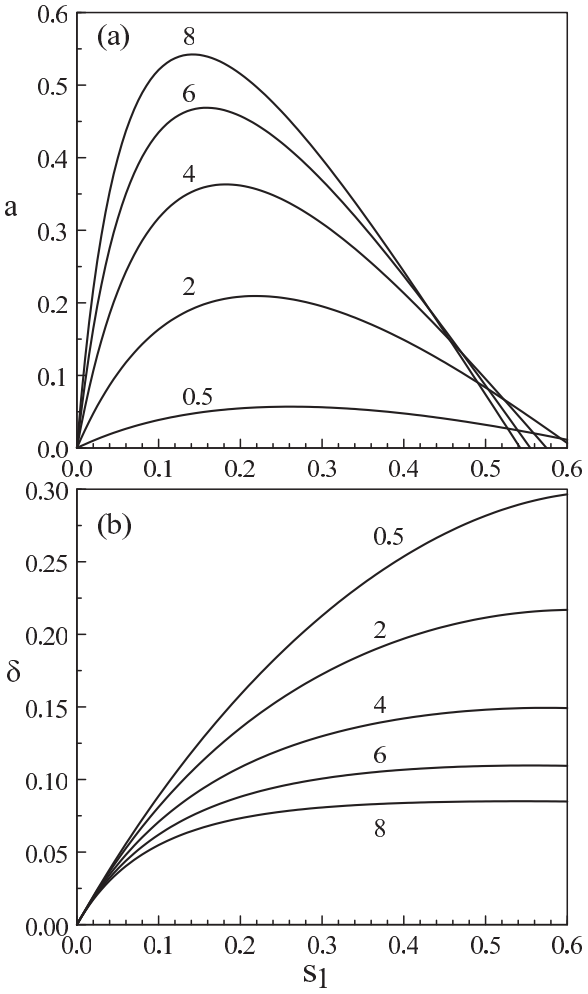

FIG. 10. Analytical solution in parametric form for $\delta = \delta(s_1)$ and $a = a(s_1)$. The labels in the figures denote the value of $\gamma = \tau/\varepsilon$. At a fixed γ, two branches of solutions for $a = a(s_1)$ emerge from a maximum as we decrease a.

for the intervals $0 < s < s_1$ and $s_1 < s < s_2$. After some simplifications, we obtain a simple expression for y_0 given by

$$y_0 = -1 + a + \frac{2s_1}{1+\delta}. \tag{45}$$

From Eq. (43b), we eliminate y_0 using Eq. (45) and obtain an equation for a as a function of s_1 and δ:

$$a = -\frac{2s_1}{1+\delta} + \frac{2 - 2\exp(-\gamma s_1)}{1 - \exp(-\gamma(1+\delta))}\exp(-\gamma\delta). \tag{46}$$

Thereby, we arrive at a solution in parametric form in dependence on the parameter s_1. We fix the delay γ and solve the quadratic Eq. (44) for $\exp(-\gamma\delta)$. This provides δ as a function of s_1 [see Fig. 10(b)]. We then determine a as a function of s_1 using Eq. (46) [see Fig. 10(a)]. Figure 9 depicts the time series for $x(s)$ and $x(s-1)$ for $a = 0.1$, $\varepsilon = 0.01$, and $\tau = 0.08$. We find $s_1^{\text{num}} = 0.486$ and $\delta^{\text{num}} = 0.083$. The analytical approximation shown in Fig. 10(a) for the line $\gamma = \tau\varepsilon^{-1} = 8$ and $a = 0.1$ gives $s_1^{\text{anal}} = 0.486$, which agrees with the numerical estimate.

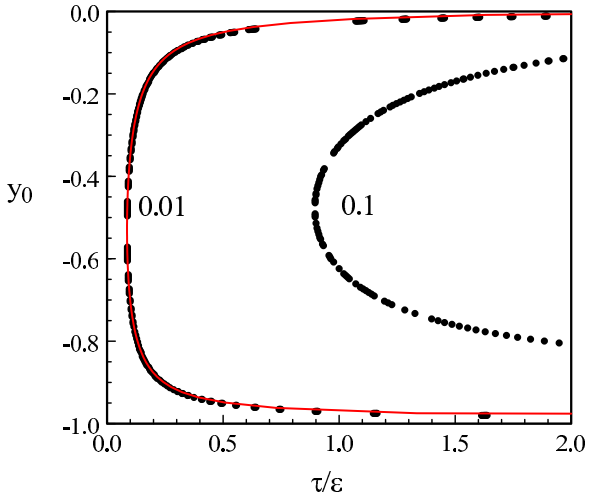

FIG. 11. Analytical bifurcation diagram for $y_0 = y_0(\tau/\varepsilon)$. The parameter a is chosen as 0.01 and 0.1 in the red (gray) and black curves, respectively.

The analytical approximation shown in Fig. 10(b) for the line $\gamma = \tau\varepsilon^{-1} = 8$ and for $s_1 = 0.486$ gives $\delta^{\text{anal}} = 0.084$, which is in good agreement with the numerical estimate.

In Fig. 11, we represent y_0 as a function of $\gamma = \tau/\varepsilon$ for two different values of a. If a becomes small, the limit point of periodic solutions approaches zero and the bifurcation diagram exhibits a boundary layer connecting two plateaus located at $y_0 = 0$ and $y_0 = 1$.

The boundary layer equations can be obtained by exploring the limit γ small keeping s_1 and δ fixed. From Eq. (44), we obtain

$$O(\gamma^2) : \delta^2 + \delta(1 - s_1) + s_1^2 - s_1 = 0 \tag{47}$$

as the leading order equation for $\gamma \to 0$. From Eq. (46), we then find

$$a = \frac{\gamma s_1}{1+\delta}(1 - \delta - s_1), \tag{48}$$

or in terms of γ for fixed a,

$$\gamma = \frac{(1+\delta)a}{s_1(1 - \delta - s_1)}. \tag{49}$$

The conditions $a > 0$, $\gamma > 0$, $\delta > 0$ define the domain in s_1 ($0 < s_1 < 2/3$). We solve Eq. (47) and determine $\delta = \delta(s_1) > 0$. We then find γ using Eq. (49) and y_0 using Eq. (45). This boundary layer solution is shown in Fig. 11 by the full line ($a = 0.01$).

V. DISCUSSION

In this paper, we have considered the FitzHugh-Nagumo model subject to delayed self-feedback in the parameter range where it admits a linearly stable steady state. We raised the question whether a stable limit-cycle solution may coexist with this stable steady state for low values of the delay τ. According to Chicone [34], small delays do not matter, if the reduced system ($\tau = 0$) is structurally stable. This is indeed the case, if the timescale separation parameter ε, measuring the fast changes of activator variable x, is kept fixed. However, the

limit $\tau \to 0$ has to be treated as a singular limit if we consider the limit $\varepsilon \to 0$ as we generally do for slow-fast systems. The perturbation analysis described in Sec. IV suggests that the coexistence of a stable time-periodic and a stable steady state appears as soon as $\tau = O(\varepsilon)$ in the limit $\varepsilon \to 0$. This was demonstrated analytically for the FHN system with threshold nonlinearity but still needs to be demonstrated for the original FHN equations for which we only have numerical evidence. Our analysis indicates that if $\tau = O(\varepsilon)$, the delayed feedback has no immediate effects on the inhibitor y but is boosting the fast changes of the activator x. As a result, sustained τ-periodic oscillations are possible under specific perturbations of the steady state. Our analysis substantiates the limit-point mechanism responsible for the birth of the stable limit cycles. We note from Fig. 11 that the time-averaged value of the inhibitor $y = y_0$ for the upper branch of stable limit-cycles approaches zero from negative values as we increase τ/ε. This is consistent with the numerical simulations of the original FHN equations for low values of τ (see Figs. 5 and 7). On the other hand, the lower branch of unstable limit-cycles exhibits a time averaged $y = y_0$ that approaches $y = -1$, i.e., is coming close to the stable steady state $(x,y) = (-a, -1-a)$ where $a = 0.1$. This is consistent with the analysis in Sec. II, where a branch of unstable periodic solution is found to closely overlap the stable steady state.

We need to realize that novel phenomena solely induced by a delayed feedback are possible for systems as simple as the FHN equations. Traditionally, we start by determining bifurcations points of a basic steady state and we then follow the emerging branches of solutions. For the parameter values we have considered, there are no bifurcation points, and stable near τ-periodic oscillations were first found accidentally. In this paper, three distinct strategies have been developed in order to capture these periodic solutions. Each of them offer advantages and limitations. The most classical approach is to explore the bifurcation diagram of periodic solutions for parameter values close to the values of interest but where Hopf bifurcation points have been detected. A numerical continuation method then revealed the limit-point mechanism generating stable periodic solutions. The second approach is based on the construction of a limit cycle in the phase plane (x,y) valid in the limit $\varepsilon \to 0$ (τ fixed). It is not a routine application of singular perturbation techniques for slow-fast systems because some anticipation of the form of the solution is needed. By assuming that the two fast transitions layers are located at equal distance from the $y = 0$ axis, we were able to determine the bifurcation diagram analytically. This assumption is, however, no more valid if τ approaches its limit-point value τ_c. Last, we have proposed a perturbation analysis, where τ is scaled with respect to ε. The leading approximation is described by a simpler problem but is still a nonlinear delay differential equation. We solved it only for a particular form of the FHN nonlinearity.

Models describing delay-coupled oscillators are popular tools for studying different forms of neural synchrony (see Ref. [35] for a recent review). However, the network response of delayed coupled excitable units or mixed delay coupled excitable and oscillatory units deserve similar attentions. In Ref. [25], we stressed the fact that several periodic regimes of period τ/n coexisting with a stable steady state can robustly appear in a single cell. Here, we showed that a small delay is enough to generate these oscillations. Having the alternative to be steady or oscillatory, we reasonably expect distinct forms of synchronization for populations of excitable cells compared to networks of coupled oscillators.

ACKNOWLEDGMENTS

This work was supported by Deutsche Forschungsgemeinschaft in the framework of Collaborative Research Center SFB 910. L.B. and P.H. acknowledge support by BMBF (Grant No. 01Q1001B) in the framework of BCCN Berlin. L.W. acknowledges the Conseil Régional de Lorraine, FEDER through the project PHOTON, and the Agence Nationale de la Recherche (ANR) TINO project (Grant No. ANR-12-JS03-005). T.E. is grateful of the support of the F.N.R.S. This work also benefited from the support of the Belgian Science Policy Office under Grant No. IAP-7/35 photonics@be.

APPENDIX: APPROXIMATIONS OF THE FIRST HOPF BIFURCATIONS

In this Appendix, we determine the leading approximations of the first Hopf bifurcation assuming $a < 1$ and $|a-1| = O(\varepsilon)$, $\sigma = O(\varepsilon^{1/2})$, and two distinct scalings for τ.

Case 1. Introducing

$$\tau = \varepsilon\theta,\ a = 1+\varepsilon\alpha, \quad \text{and} \quad \sigma = \varepsilon^{-1/2}\omega$$

into Eqs. (3a) and (3b) leads to the following simplifications:

$$-\omega^2 - \varepsilon^{-1/2}\omega c(\varepsilon^{1/2}\omega\theta + ...) + 1 = 0,$$

$$-2\varepsilon\alpha + ... - \varepsilon c\frac{\omega^2\theta^2}{2} + ... = 0.$$

The leading order equations are given by

$$-\omega^2(1+c\theta) + 1 = 0,$$

$$-2\alpha - c\frac{\omega^2\theta^2}{2} = 0,$$

from which we obtain ω^2 and α as

$$\omega^2 = \frac{1}{1+c\theta} \text{ and } \alpha = -\frac{c\theta^2}{4(1+c\theta)}.$$

Case 2. Introducing

$$\tau = \varepsilon^{1/2}\theta,\ \sigma = \varepsilon^{-1/2}(\sigma_0 + \varepsilon^{1/2}\sigma_1 + ...), \quad \text{and} \quad a = 1+\varepsilon\alpha,$$

where

$$\sigma_0\theta = 2n\pi\ (n = 1,2,...),$$

now leads to the following equations relating σ_1 and α:

$$-\sigma_0^2 - \sigma_0 c\sigma_1\theta + 1 + ... = 0,$$

$$-\alpha - c\frac{\sigma_1^2\theta^2}{4} + ... = 0,$$

from which we find

$$\alpha = -\frac{(1-\sigma_0)^2}{4\sigma_0^2 c}, \quad \sigma_1 = \frac{1-\sigma_0^2}{\sigma_0 c\theta}.$$

[1] J. Keener and J. Sneyd, *Mathematical Physiology*, Interdisciplinary Applied Mathematics (Springer, Berlin, 1998).

[2] C. Fall, E. Marland, J. Wagner, and J. Tyson, eds., *Computational Cell Biology*, Interdisciplinary Applied Mathematics, Vol. 20 (Springer-Verlag, New York, 2002).

[3] G. B. Ermentrout and D. H. Terman, *Mathematical Foundations of Neuroscience*, Vol. 35 (Springer Science & Business Media, New York, 2010).

[4] A. L. Hodgkin and A. F. Huxley, J. Physiol. **117**, 500 (1952).

[5] R. FitzHugh, Biophys. J. **1**, 445 (1961).

[6] J. Nagumo, S. Arimoto, and S. Yoshizawa, Proc. IRE **50**, 2061 (1962).

[7] E. Schöll, G. Hiller, P. Hövel, and M. A. Dahlem, Philos. Trans. R. Soc. London A: Mathematical, Physical and Engineering Sciences **367**, 1079 (2009).

[8] B. Hauschildt, N. B. Janson, A. Balanov, and E. Schöll, Phys. Rev. E **74**, 051906 (2006).

[9] P. Hövel, M. A. Dahlem, and E. Schöll, Int. J. Bifurcat. Chaos **20**, 813 (2010).

[10] A. Panchuk, D. P. Rosin, P. Hövel, and E. Schöll, Int. J. Bifurcat. Chaos **23**, 1330039 (2013).

[11] W. J. Freeman, Int. J. Bifurcat. Chaos **10**, 2307 (2000).

[12] A. Keane, T. Dahms, J. Lehnert, S. A. Suryanarayana, P. Hövel, and E. Schöll, Eur. Phys. J. B **85**, 407 (2012).

[13] V. Vuksanović and P. Hövel, Chaos **25**, 023116 (2015).

[14] G. Deco, V. Jirsa, A. McIntosh, O. Sporns, and R. Kötter, Proc. Natl. Acad. Sci. USA **106**, 10302 (2009).

[15] G. Deco and V. K. Jirsa, J. Neurosci. **32**, 3366 (2012).

[16] R. Ton, G. Deco, and A. Daffertshofer, PLoS Comput. Biol. **10**, e1003736 (2014).

[17] C. Cakan, J. Lehnert, and E. Schöll, Eur. Phys. J. B **87**, 54 (2014).

[18] P. Hövel, *Control of Complex Nonlinear Systems with Delay* (Springer Science & Business Media, New York, 2010).

[19] L. Weicker, T. Erneux, D. P. Rosin, and D. J. Gauthier, Phys. Rev. E **91**, 012910 (2015).

[20] G. Giacomelli, F. Marino, M. A. Zaks, and S. Yanchuk, Europhys. Lett. **99**, 58005 (2012).

[21] N. Burić and D. Todorović, Phys. Rev. E **67**, 066222 (2003).

[22] M. A. Dahlem, G. Hiller, A. Panchuk, and E. Schöll, Int. J. Bifurcat. Chaos **19**, 745 (2009).

[23] O. Vallès-Codina, R. Möbius, S. Rüdiger, and L. Schimansky-Geier, Phys. Rev. E **83**, 036209 (2011).

[24] L. Weicker, T. Erneux, L. Keuninckx, and J. Danckaert, Phys. Rev. E **89**, 012908 (2014).

[25] L. Weicker, L. Keuninckx, G. Friart, J. Danckaert, and T. Erneux, in *Control of Self-Organizing Nonlinear Systems*, Understanding Complex Systems, edited by E. Schöll, S. H. L. Klapp, and P. Hövel (Springer International Publishing, New York, 2016), pp. 337–354.

[26] H. Smith, *An Introduction to Delay Differential Equations with Applications to the Life Sciences*, Vol. 57 (Springer Science & Business Media, New York, 2010).

[27] R. E. Plant, SIAM J Appl. Math. **40**, 150 (1981).

[28] T. Prager, H.-P. Lerch, L. Schimansky-Geier, and E. Schöll, J. Phys. A: Math. Theoret. **40**, 11045 (2007).

[29] N. B. Janson, A. G. Balanov, and E. Schöll, Phys. Rev. Lett. **93**, 010601 (2004).

[30] A. Balanov, N. B. Janson, and E. Schöll, Physica D: Nonlin. Phenom. **199**, 1 (2004).

[31] M. Krupa and J. D. Touboul, J. Nonlinear Sci. **26**, 43 (2015).

[32] The FHN equations analyzed in Ref. [31] can be reformulated in the form of our FHN equations by changing $y \to -y$, $a \to -a$, $t \to \varepsilon t$, and $J = -c$.

[33] K. Engelborghs, T. Luzyanina, and G. Samaey, *DDE-BIFTOOL v. 2.00: A Matlab package for bifurcation analysis of delay differential equations*, Tech. Rep. TW-330 (Department of Computer Science, K. U. Leuven, Belgium, 2001).

[34] C. Chicone, J. Diff. Equ. **190**, 364 (2003).

[35] P. Ashwin, S. Coombes, and R. Nicks, J. Math. Neurosci. **6**, 2 (2016).